Available online at www.sciencedirect.com
SCIENCE DIRECT®
PERGAMON
International Journal of Heat and Mass Transfer 46 (2003) 3109–3117
International Journal of HEAT and MASS TRANSFER
www.elsevier.com/locate/ijhmt

Natural convection heat transfer increase at the laminar–turbulent transition in the presence of instationary longitudinal vortices

R. Biertümpfel [a,*], H. Beer [b]

[a] Schott Glas, Hattenbergstraße 10, 55014 Mainz, Germany
[b] Institut für Technische Thermodynamik, Technische Universität Darmstadt, Petersenstraße 30, 64287 Darmstadt, Germany

Received 23 October 2002

Abstract

Heat transfer of a liquid to a solid wall in natural convection is studied in the regime of laminar to turbulent transition in the presence of longitudinal vortices. These vortices lead to an increase in heat transfer, especially in their later stage before breakdown. This last increase is significant and even higher than one would expect for a turbulent flow. In this work heat transfer was studied numerically and in experiments using thermochromic liquid crystals.

Keywords: Natural convection; Heat transfer; Transition; Longitudinal vortices; Thermochromic liquid crystals

1. Introduction

Heat transfer of fluids to solid walls has been studied in numerous different papers, and it is well known that the heat transfer depends strongly on the state of the flow. Although there are analytical solutions for laminar flows, only empirical correlations for the heat transfer in the turbulent regime exist. In the present study, heat transfer in the transition region between laminar and turbulent flow of natural convection at an inclined flat wall is examined. Vliet [12] and Shaukatullah and Gebhardt [10] had already performed experiments for this type of flow. Vliet [12] found a correlation for the mean heat transfer as a function of the downstream position (see Eq. (7)) with the heat transfer being much higher than for laminar flow. However, there is a tremendous scatter in the measured values for the transition region.

The experiments of Sparrow and Husar [11] showed the existence of longitudinal vortices in natural convection flows at inclined walls, and Shaukatullah and Gebhardt [10] proved that these vortices have a significant influence on the local heat transfer distribution during the laminar–turbulent transition. Due to the limits of their measurement technique using thermocouples, quantitative results for the heat transfer could not be made, however, the data of Shaukatullah and Gebhardt [10] give already a small hint that the heat transfer at the end of transition is higher than expected. This increase in heat transfer is strongly coupled to the evolution of the longitudinal vortices. Zuercher et al. [15] reported a significant increase in vorticity just before the longitudinal vortices decay into turbulence.

Heat transfer measurements in similar flows with longitudinal vortices show the same evidence. For forced convection above a heated flat plate (Blasius-boundary layer) Imura et al. [3] state a significant increase and scatter of the measured values before the heat transfer reaches constant values in the turbulent regime. At the edges of heated flat plates the natural convection flow develops longitudinal vortices as well. The data of Kitamura and Kimura [8] show a significant increase in heat transfer at the end of lifetime of the longitudinal vortices.

* Corresponding author.
E-mail addresses: ralf.biertuempfel@schott.com (R. Biertümpfel), beer@ttd.tu-darmstadt.de (H. Beer).

0017-9310/03/$ - see front matter © 2003 Elsevier Science Ltd. All rights reserved.
doi:10.1016/S0017-9310(03)00079-6

Nomenclature

A	shape function of a wave like disturbance
c	propagation velocity
g	gravitational acceleration
Gr^*	modified Grashof number for constant heat flux
h	local heat transfer coefficient
k	thermal conductivity
Nu	Nusselt number
Pr	Prandtl number
$\dot{q}$	constant heat flux
Ra^*	modified Rayleigh number for constant heat flux
T_{wall}	measured local temperature of the plate
T_∞	far field temperature of the ambient fluid
v	vector of a small disturbance (velocity, pressure, temperature)
X	a given downstream position
x	downstream direction of the coordinate system
y	wall normal direction of the coordinate system
z	transverse direction of the coordinate system

Greek symbols

α	dimensionless wave number
β	coefficient of thermal expansion
γ	inclination of the wall against the vertical
λ_1	wavelength of the primary instability
λ_x	wavelength of the secondary instability
ν	viscosity
σ	dimensionless wave propagation

Subscripts

1	primary instability
x	in downstream direction or at a given position X

1.1. Geometry of the flow

Fig. 1 shows the basic set-up of the flow. In this study we consider a heated semi-infinite flat plate, which is located in a fluid at rest. The flat plate has an edge (at $x=0$) and is infinite in the z-direction. The y-direction is perpendicular to the flat plate and gives the distance to the wall.

Because of the plate being inclined against the vertical by a small angle γ, a natural convection flow develops which is two-dimensional and laminar at the beginning. But a little bit downstream the flow becomes unstable to three-dimensional longitudinal vortices, see [4,7]. These vortices are pair wise counter-rotating and their rotation axis is parallel to the main flow direction (x-direction). That means the boundary layer flow is doing a more screw-like motion in x-direction. The vortices are steady and growing in the downstream direction.

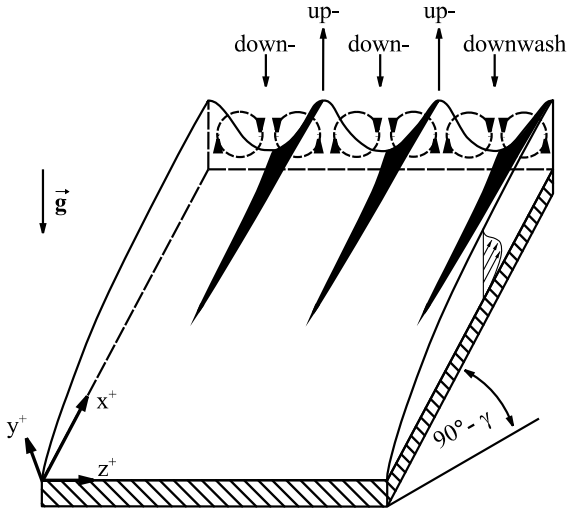

Fig. 1. Flow geometry of longitudinal vortices in natural convection at an inclined wall.

Due to these vortices the boundary layer is deformed and regions of strong up- and down-wash develop, which effect the heat transfer significantly, see [4]. This change of the 2D laminar flow to a 3D laminar flow with longitudinal vortices is known as primary instability, or in the case of forced flow over concave surfaces as 'Görtler instability', see [2].

As these laminar vortices grow stronger, they initiate the laminar–turbulent transition and in their later stage they become unsteady and start a wavy, sinuous-like motion, which is called secondary instability. The wavy motion of the longitudinal vortices grows very fast with the downstream flow and finally the vortices break up into turbulence. During the last stage of the secondary instability the mean heat transfer of the flow is increased strongly, and with the break up of the vortices the heat transfer ceases to turbulent values.

2. Experimental set-up

The aim of the experiments was, to investigate the character of the secondary instabilities and to measure the heat transfer during laminar–turbulent transition.

Therefore, a constant heat flux plate (31.5 mm wide and 49.5 mm long) inside a 100 l water tank was examined, using 'thermochromic liquid crystals (TLC)' to monitor the surface temperatures. The experimental set-up used is already described in detail in the papers of Jeschke et al. [5,6].

2.1. Heat transfer measurement

The TLC-method visualizes the surface temperature of the inclined heated plate with a resolution of 50 μm. This allows to measure a fine grained surface temperature distribution of a large area, that opens the possibility to calculate exact values for the mean heat transfer (in the transverse direction). The dimensionless heat transfer is expressed by the Nusselt number, which can be expressed for a constant heat flux plate as follows:

$$Nu = \frac{hx}{k} = \frac{\dot{q}}{T_{\text{wall}} - T_{\infty}} \frac{x}{k} \tag{1}$$

2.2. The character of the secondary instability

The longitudinal vortices have a strong influence on the heat transfer, thus, the pattern of local temperatures on the hot plate (which is visualized by TLC) is a 'footprint' of the vortices itself. This means that in the down-wash region of each vortex pair the heat transfer is enhanced, leading to a lower surface temperature, however, in the up-wash region of the vortex pair the temperature is high, because the heat transfer is decreased. Thus, a steady vortex is visualized by the TLC as a steady pattern of lines along the downstream direction. As soon as the secondary instability sets in, the longitudinal vortices become unsteady and move in a wavy, sinuous manner as a function of time. Fig. 2 (left side) gives a sketch of the longitudinal axis of such vortices. Further downstream the wavy motion increases in amplitude, but the wavelength λ_x or the velocity c of the motion does not change. The secondary motion is easily visualized by TLC and can be examined using a CCD-camera and image processing software, see [1].

The character of the secondary instabilities is described by three parameters: the wavelength λ_x of the sinuous motion, the velocity c of the moving wave and the growth rate of the developing amplitude.

The wavelength λ_1 resembles the interval between the longitudinal vortex pairs of the primary instability. This primary wavelength remains constant even when the vortex pair gets instable to the secondary instability.

2.2.1. Image analysis

In order to measure growth rate, wavelength and propagation velocity of the secondary instability, colour pictures of the TLC were taken. Then an image analysis procedure was used, that extracted the trace of the high temperature regions (which is equivalent to the up-wash regions of the longitudinal vortices). The obtained result is a good measure for the vortex axis of a longitudinal vortex pair. Such a trace is shown in Fig. 2, right side. By using a fast-Fourier-transform (FFT) algorithm the wavelength λ_x of the secondary motion of the longitudinal vortices could be found. A dimensionless wave number α_x can then be calculated:

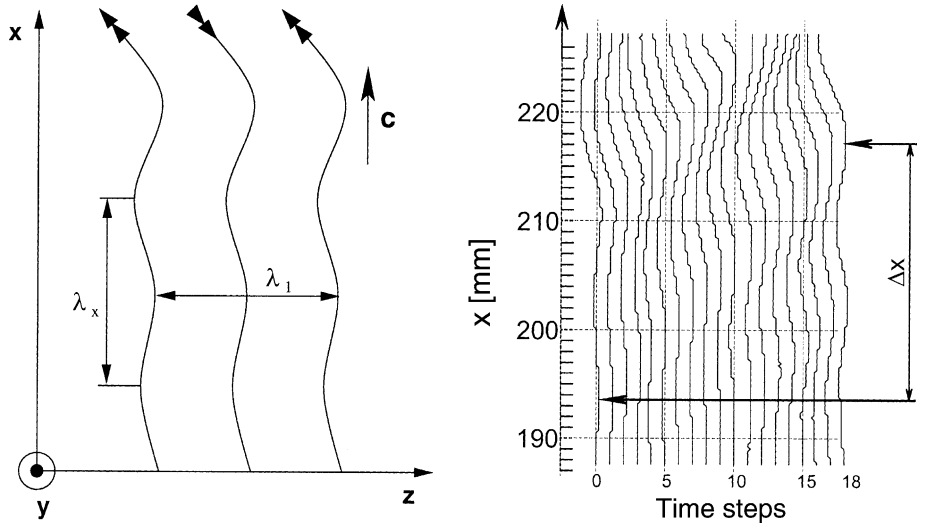

Fig. 2. (Left) Sketch of the vortex axis of three longitudinal vortices that are unstable to secondary instabilities. This secondary instability is a wavy motion of the longitudinal vortex, which has a wavelength of λ_x and that propagates downstream with velocity c. (Right) Image analysis of the measurement of a vortex pair at 18 succeeding time steps. The wavy structure and the propagation in downstream direction of the secondary instability can clearly be seen. The velocity c is calculated by $c = \Delta x/\Delta t$.

$$\alpha_x = \frac{2\pi}{\lambda_x}\frac{X}{(Gr_x^*)^{0.2}} \tag{2}$$

with X being the downstream position and Gr_x^* is the Grashof number for an inclined constant heat flux plate, defined by

$$Gr_x^* = \frac{g\cos(\gamma)\beta\dot{q}X^4}{k\nu^2} \tag{3}$$

The propagation velocity c of the longitudinal vortices was measured by tracking the peak or the valley of the sinuous wave of the vortex axis, as shown on the right side of Fig. 2. For each vortex pair several peaks/valleys were tracked and then averaged. Then the dimensionless wave propagation σ_x can be derived by:

$$\sigma_x = \frac{2\pi c}{\lambda_x}\frac{X^2}{\nu(Gr_x^*)^{0.6}} \tag{4}$$

2.3. Flow visualization

Investigating the local surface temperature distribution is very useful in order to examine the behaviour of the secondary instabilities. However, it is not a proof for the one and only existence of longitudinal vortices. Therefore, the flow was visualized independently by two different techniques: First, an electrochemical technique using thymol blue as a dye, and second, particle image velocimetry (PIV). A detailed description of the set-up is given by Biertümpfel [1].

3. Numerical simulation

In addition to the experiments the flow field has been modelled by a numerical simulation of the boundary layer. In order to reduce the computational time, only a single vortex pair was considered. The computed domain of the flow was restricted to the region of the laminar–turbulent transition (see Fig. 3). The size of the grid was 33 cells in x-, 20 cells in y- and 33 cells in z-direction. The cells were equidistant in x- and z-direction, but a refinement was applied in y-direction. E is the entrance region of the flow. The width of the domain covers one longitudinal vortex pair. In the downstream direction the domain starts in the region of steady laminar longitudinal vortex flow and it ends at the turbulent flow regime. In the direction perpendicular to the wall (y) it covers the whole boundary layer. The boundary conditions at the entrance region (E) were set to the flow field condition of a laminar longitudinal vortex pair (primary instability). The values were taken from the calculations by Jeschke [4]. Additionally, the values of this inflow condition were distorted by a small periodic disturbance in order to model an infinite small

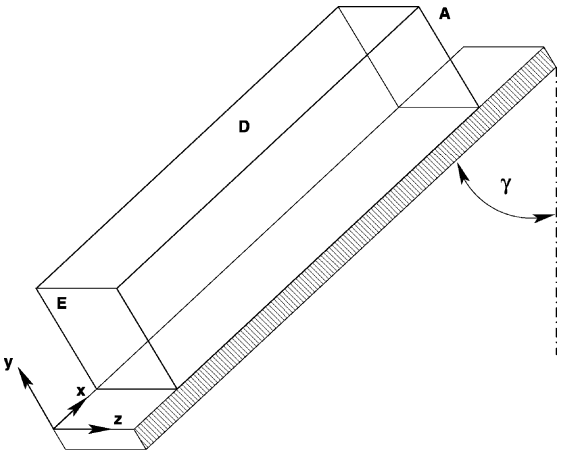

Fig. 3. Computational domain of the numerical simulation.

disturbance that is amplified by the primary flow. This disturbance **v** is a wave-like motion of the form:

$$\mathbf{v} = \mathbf{A}(y,z)\mathrm{e}^{\alpha x-\sigma t} \tag{5}$$

The values of **A**, σ and α were taken from a stability analysis by Biertümpfel [1]. The results of this stability analysis had been confirmed by the experimental findings of this study. The origin of such disturbances is not known, but it is believed that these disturbances are present and that the primary flow will amplify only one significant type of disturbance, which will result in the secondary instability further downstream. A more detailed discussion may be found in [1,13,14].

At the sides of the computational domain, the transverse direction of the flow, periodic boundary conditions were applied, and on top of the computational domain (D), the far field condition of the laminar 2D-flow was chosen as boundary condition. The outlet (A) was set to a free, no-influence boundary condition.

The code FLUENT was used to solve the Navier–Stokes' and the energy equation presuming Boussineq's approximation. For details the reader is referred to [1].

The aim of the numerical simulation was to give answers to the following questions: Is there a second proof for the existence of secondary instabilities of longitudinal vortices, or is the observed motion just a result of the experimental apparatus? Secondly, can the heat transfer be calculated for the laminar–turbulent transition?

4. Results and discussion

4.1. Results of the flow visualization

Fig. 4 shows photographs of the top view of the flow along the wall. The flow is visualized using thymol blue

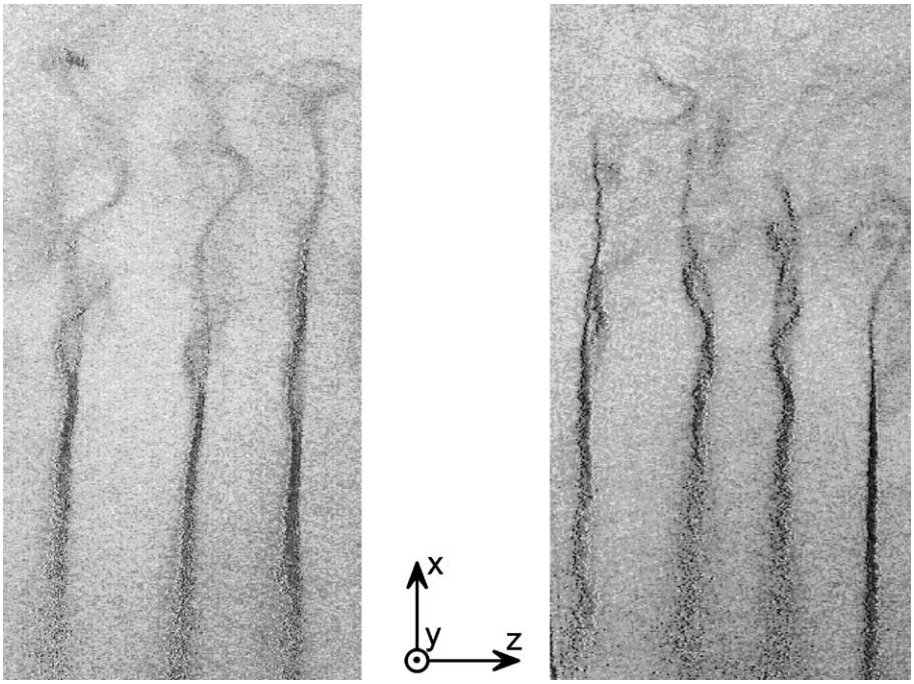

Fig. 4. Flow visualization using thymol blue. The view is out of the far field perpendicular to the wall (comparable to Fig. 2). On the left a sinuous motion is shown and on the right a varicose motion of the secondary instabilities is depicted.

as a dye indicating the wavy movement of the longitudinal vortices. Fig. 4 (left) elucidates a so called 'sinuous' mode of oscillating vortex pairs and Fig. 4 (right) states a so called 'varicose' mode [13,14].

Fig. 5 gives the results of a PIV-measurement of the cross-section of a single vortex pair: The main flow is streaming into the page and the heated flat plate is located at the bottom of the diagram. The isolines show the rotation of the vortex pair. Although, this picture does not show the time dependent movement of the secondary instability, it states the existence of regular longitudinal and counter-rotating vortex pairs.

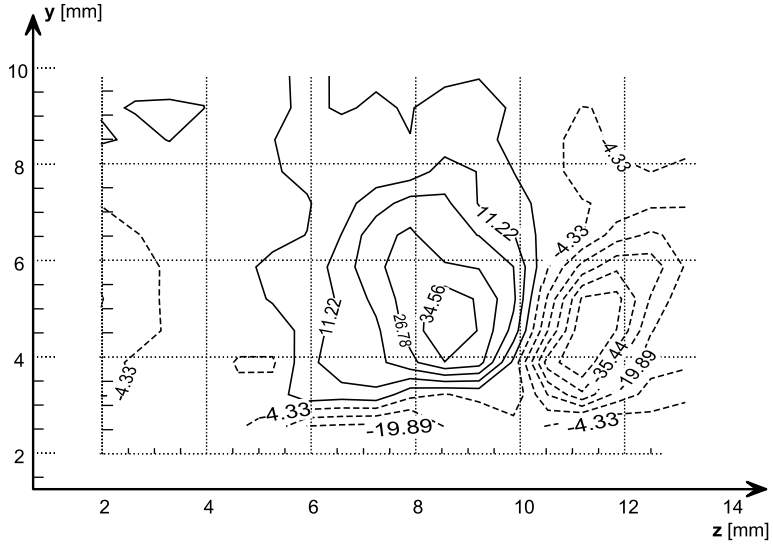

Fig. 5. Shown is a result of PIV: Circulation in the cross-sectional plane of a vortex pair. The wall is at the bottom of the figure, and on top there is the far field.

All these results reveal that only longitudinal vortex pairs are present. Thus, the TLC visualization of local surface temperatures gives an exact description of the longitudinal vortices, which creates any of the observed structures.

The wavy motion of the longitudinal vortices also has been visualized applying a direct numerical simulation (DNS), see [1]. For the DNS a fluid of Prandtl number $Pr = 1$ was used and the calculation was done for a smaller cavity than in the experiments (for the reason of reduction of computational time). The results of the simulation correspond to the experimental findings: Although the wavelengths and velocities of the secondary instabilities are different in simulation and experiment (due to different fluids), a development of longitudinal vortices with secondary instabilities could be observed.

4.2. Characteristic parameters of secondary instabilities

Basically the secondary instabilities can be described by three parameters (see Eq. (5)): (a) the growth rate of the amplitude of oscillation, (b) the wavelength λ_x or the dimensionless wave number α_x, and (c) the travelling velocity c of the wave or the dimensionless wave propagation σ_x.

4.2.1. Growth rate

The growth of the secondary instabilities is very fast: Usually the vortex pair oscillates only a few wavelengths before breakdown occurs. Thus, it was not possible to identify any law for the growth: some of the results lead to the assumption of linear, others to exponential growth. Therefore, the growth rate was not studied any further, because a common rule for the growth could not be found nor could any measure for the growth be given.

In the linear stability analysis usually an exponential law for the growth is assumed [1,13,14]. This assumption is justified for the purpose of the linear stability analysis, which considers only very small disturbances. However, in an experiment only instabilities of a developed state can be observed, and the law of growth in such a largely developed secondary instability may be very different from the initial exponential growth.

4.2.2. Wave number α_x

In Fig. 6 the distribution of the measured wavelength is shown in terms of the dimensionless wave number α_x

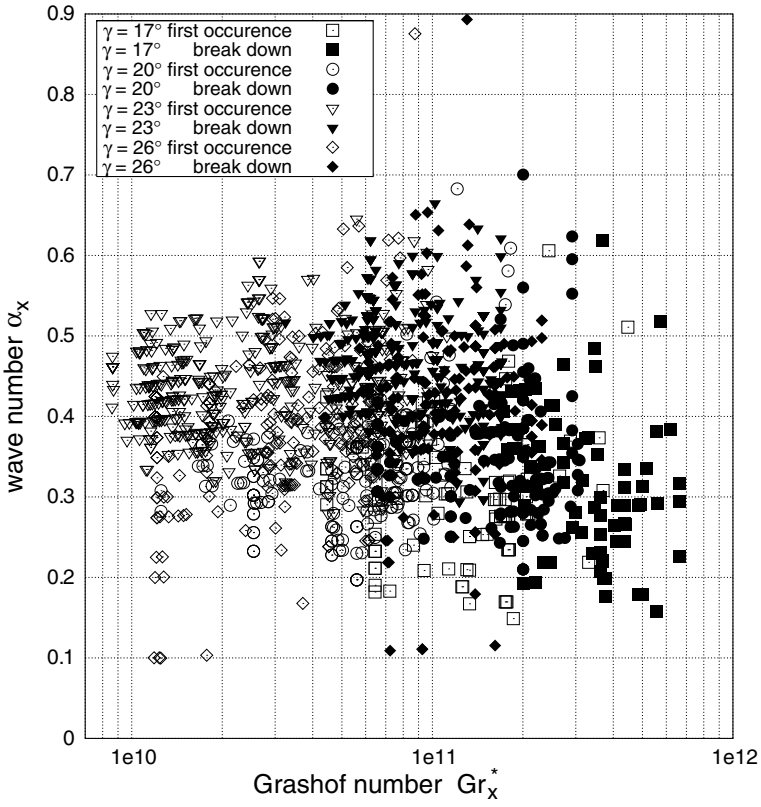

Fig. 6. Distribution of wave number α_x at four different angles of inclination.

as a function of the modified Grashof number Gr_x^*, which is a measure for the downstream position X.

Because all dimensionless numbers use the downstream position X for the scaling, the results of a single longitudinal vortex are plotted twice: Once for the position X of the first occurrence of the secondary instability and secondly for the breakdown position of the longitudinal vortex. The actual (dimensional) wavelength λ_x remained constant from the onset of the instability until breakdown.

It is remarkable that all wave numbers α_x of the secondary instability are of the same order of magnitude.

4.2.3. Propagation velocity of the secondary instability

Just like the wavelength λ_x, the propagation velocity c did not change. Fig. 7 depicts the dimensionless propagation σ_x of the secondary instability. The error bars in the horizontal direction show the length of the secondary instability from the first detectable occurrence until the breakdown of the vortex. The vertical error bar states the standard deviation of the measurement.

Again, the order of magnitude of the measurements is the same and the obtained results are almost similar.

4.3. Heat transfer

For the laminar regime one can derive an analytical solution for the heat transfer (of water), see [1,9]:

$$Nu_{\text{laminar}} = 0.58427(Ra_x^*)^{0.2} \quad \text{for } Pr = 5.414 \tag{6}$$

Vliet [12] was able to show that the mean heat transfer in the turbulent region is well described by the relation:

$$\overline{Nu}_{\text{laminar}} = 0.302(Ra_x^*)^{0.24} \tag{7}$$

with $\overline{Nu} = (\bar{h}X/k) = (X/k)(1/(z_2 - z_1)) \int_{z_1}^{z_2} h\,dz$ being the Nusselt number for the in transverse (z-)direction averaged heat transfer for a given downstream position X. For flow fields with constant heat flux $\dot{q}$ the Rayleigh number Ra^* and the Grashof number Gr^* are defined by:

$$Ra_x^* = Gr_x^* Pr = \frac{g\cos(\gamma)\beta\dot{q}X^4}{\nu} \tag{8}$$

In Fig. 8 the results of the heat transfer measurement are shown. The thick bunch of lines in the middle depict the Nusselt number averaged in the transverse (z-)direction. These lines represent 40 measurements of succeeding time steps ($\Delta t = 200$ ms). The line below depicts the minimum values that are archived in the up-wash regions of the vortex pairs and the upper line gives the maximum values that are reached in the down-wash regions of the vortex pairs. (Error bars indicate the uncertainty of the measurement.)

As expected the measured heat transfer corresponds to the predicted laminar values for low Grashof numbers when the longitudinal vortices are weak. But for rising Grashof number (or higher downstream position) the longitudinal vortices grow stronger and increase the

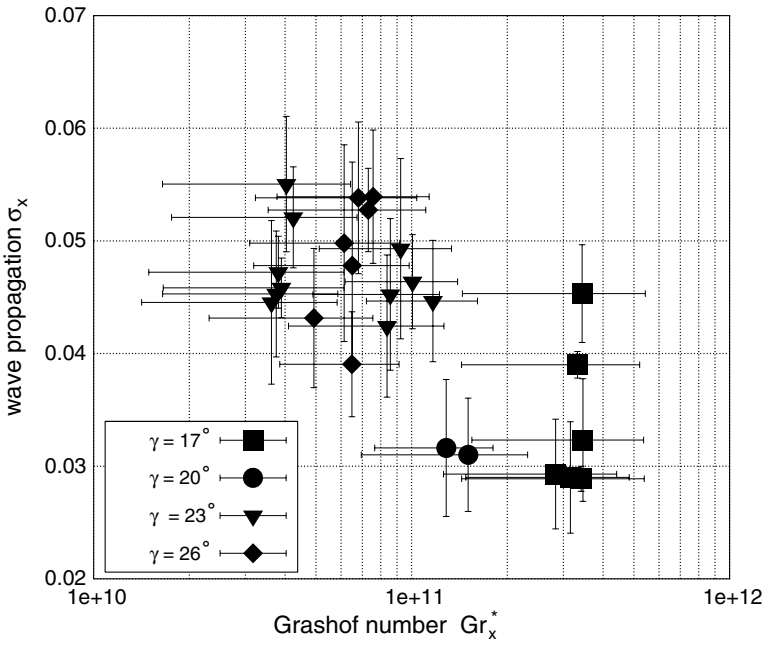

Fig. 7. Propagation velocity σ_x for four angles of inclination.

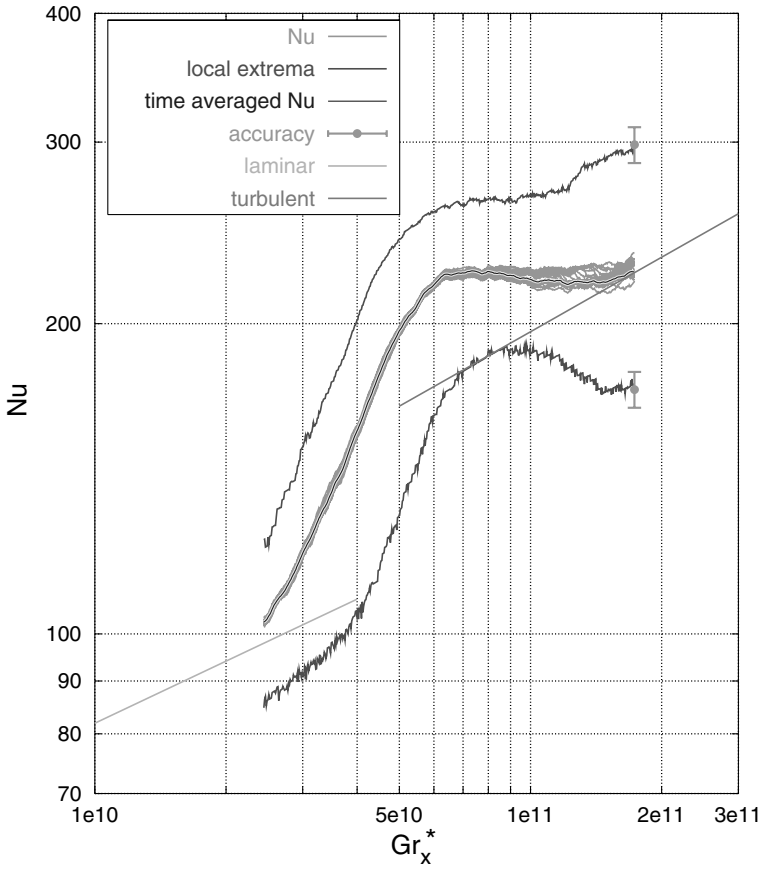

Fig. 8. Heat transfer at an inclined hot plate. Inclination $\gamma = 26°$ against the vertical; $Pr = 5.414$; constant heat flux $\dot{q} = 3380$ W/m^2.

heat transfer, see [4]. Further downstream the secondary instabilities occur and start to grow very fast. The heat transfer increases much more than expected and exceeds even the turbulent values. Although the longitudinal vortices are in an unsteady motion due to the secondary instabilities, the heat transfer, which is averaged in the transverse direction, does not exhibit any dependence on time. (A time-dependence sets in when the flow changes to turbulent motion further downstream.) At their summit the secondary instabilities are so strong that the longitudinal vortices mix with each other and the flow breaks down into a turbulent motion. The heat transfer decreases and approaches the values of the turbulent correlation of Vliet.

A comparison of the experimental results with the numerical simulation shows only a qualitative agreement, see Fig. 9: Although the simulation of the boundary layer [1] reveals the same phenomena, the effect of "overshooting" occurs further downstream. This is believed to be due to the starting condition taken from [4] and to the rough numerical model, which must be improved.

The aim, however, to verify numerically the existence of an "overshooting" of the heat transfer was attained.

4.4. Discussion of the heat transfer

It is well known that longitudinal vortices influence the heat transfer significantly [4,10], however, the high increase on heat transfer in the presence of the secondary instability and the following decrease to turbulent values is a remarkable new result of this study. Jeschke [4] has already seen this effect in his measurements. Shaukatullah and Gebhardt [10] used thermocouples to investigate the longitudinal vortices, which limited the resolution of their heat transfer measurements. However, their data exhibit a much higher scatter in the region of the secondary instability and the heat transfer is well above of the turbulent correlation.

Similar effects can be found for other flows with longitudinal vortices: The heat transfer data of Imura et al. [3] for forced convection at the horizontal plate and of Kitamura and Kimura [8] for natural convection at the horizontal plate show an increase in heat transfer

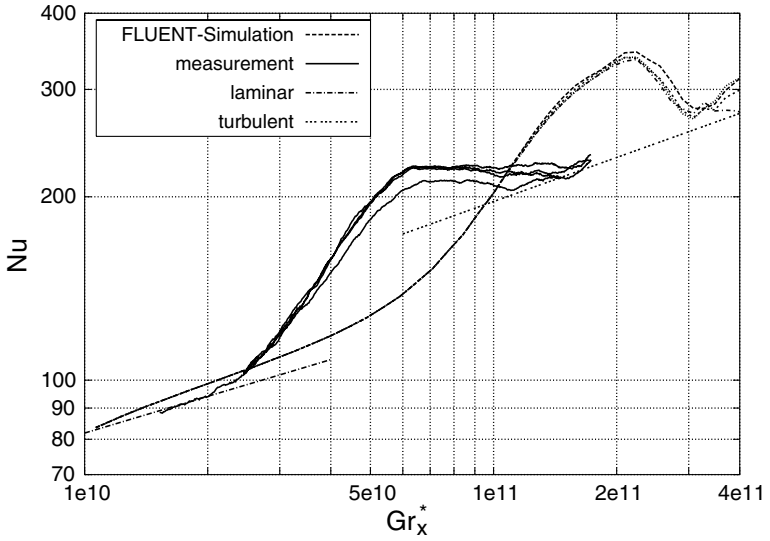

Fig. 9. Heat transfer measurement and numerical simulation.

above turbulent values for the regime of longitudinal vortices before breakdown into turbulence.

A detailed analysis of the basic physical phenomenon, however, was not available so far.

References

[1] R. Biertümpfel, Längswirbelinstabilitäten 2, Ordnung und Wärmeübertragung am Übergang laminar/turbulent bei natürlicher Konvektion an der geneigten Platte, Ph.D. thesis, Technische Universität Darmstadt, Fortschritt Berichte VDI, 2001, ISBN 3-18-343107-6.

[2] J.M. Floryan, On the Görtler instability of boundary layers, Prog. Aerospace Sci. 28 (1991) 235–271.

[3] H. Imura, R.R. Gilpin, K.C. Cheng, An experimental investigation of heat transfer and buoyancy induced transition from laminar forced convection to turbulent free convection over a horizontal isothermally heated plate, ASME J. Heat Transfer 100 (1978) 429–434.

[4] P. Jeschke, H. Beer, Longitudinal vortices in a laminar natural convection boundary layer flow on an inclined flat plate and their influence on heat transfer, J. Fluid Mech. 432 (2001) 313–339.

[5] P. Jeschke, R. Biertümpfel, H. Beer, Visualization of longitudinal vortices and surface temperatures in a natural convection experiment, Proceedings Eighth International Symposium on Flow Visualization, Sorrento, Italy 1998.

[6] P. Jeschke, R. Biertümpfel, H. Beer, Liquid-crystal thermography for heat-transfer measurements in the presence of longitudinal vortices in a natural convection flow, Meas. Sci. Technol. 11 (2000) 447–453.

[7] K. Kirchgässner, Einige Beispiele zur Stabilitätstheorie von Strömungen an konkaven und erwärmten Wänden, Ingenieur-Archiv 31 (1962) 115–124.

[8] K. Kitamura, F. Kimura, Heat transfer and fluid flow of natural convection adjacent to upward-facing horizontal plates, Int. J. Heat Mass Transfer 38 (17) (1995) 3149–3159.

[9] S. Ostrach, An analysis of free-convection flow and heat transfer about a flat plate parallel to the direction of the generating body force, NACA Tech. Notes 2635 (1952) 1–47.

[10] H. Shaukatullah, B. Gebhart, An experimental investigation of natural convection flow on an inclined surface, Int. J. Heat Mass Transfer 21 (1978) 1481–1490.

[11] E.M. Sparrow, R.B. Husar, Longitudinal vortices in natural convection flow on inclined plates, J. Fluid Mech. 37 (2) (1969) 251–255.

[12] G.C. Vliet, Natural convection local heat transfer on constant-heat-flux inclined surfaces, Trans. ASME: J. Heat Transfer (1969) 511–516.

[13] X. Yu, J.T.C. Liu, The secondary instability in Goertler flow, Phys. Fluids A 3 (8) (1991) 1845–1847.

[14] X. Yu, J.T.C. Liu, On the mechanism of sinous and varicose modes in three-dimensional viscous secondary instability of Görtler rolls, Phys. Fluids A 6 (2) (1994) 736–750.

[15] E.J. Zuercher, J.W. Jacobs, C.F. Chen, Experimental study of the stability of boundary-layer flow along a heated inclined plate, J. Fluid Mech. 367 (1998) 1–25.